

Deep residual learning in CT physics: scatter correction for spectral CT

Shiyu Xu*, Peter Prinsen, Jens Wiegert and Ravindra Manjeshwar

Abstract—Recently, spectral CT has been drawing a lot of attention in a variety of clinical applications primarily due to its capability of providing quantitative information about material properties. The quantitative integrity of the reconstructed data depends on the accuracy of the data corrections applied to the measurements. Scatter correction is a particularly sensitive correction in spectral CT as it depends on system effects as well as the object being imaged and any residual scatter is amplified during the non-linear material decomposition. An accurate way of removing scatter is subtracting the scatter estimated by Monte Carlo simulation. However, to get sufficiently good scatter estimates, extremely large numbers of photons is required, which may lead to unexpectedly high computational costs. Other approaches model scatter as a convolution operation using kernels derived using empirical methods. These techniques have been found to be insufficient in spectral CT due to their inability to sufficiently capture object dependence. In this work, we develop a deep residual learning framework to address both issues of computation simplicity and object dependency. A deep convolution neural network is trained to determine the scatter distribution from the projection content in training sets. In test cases of a digital anthropomorphic phantom and real water phantom, we demonstrate that with much lower computing costs, the proposed network provides sufficiently accurate scatter estimation.

Index Terms—CT imaging, convolutional neural network, deep residual learning, material decomposition, monochromatic images, spectral CT, scatter correction.

I. INTRODUCTION

SPECTRAL CT provides additional information, on top of conventional CT, enabling more accurate diagnostics [1]. The spectral results are divided into several categories: virtual monochromatic images enabling reduced image artifacts and enhancement of contrast; material separation such as water - Iodine, Calcium - Iodine, Calcium - uric-acid; material characterization such as effective atomic number. However, there are several limitations of current spectral systems, such as inaccurate material separation and unstable image quality (IQ) which are driven by small inaccuracies in scanner calibration and data corrections. The residual errors, which are not so impactful in conventional CT, are amplified during the non-linear material decomposition in the Spectral CT image chain [2]. Scatter correction is a particularly sensitive correction in spectral CT as it depends on system effects as well as the object being imaged. The subtle residual scatter does matter regardless of whether projection-based decomposition or image-based decomposition is performed.

There are many scatter compensation techniques. An anti-scatter grid could dramatically reduce the large angle scatter signal but could also decrease primary signal and insufficiently filter out small angle scatter and multi-scatter. The most efficient way to estimate scatter is a model-based method that defines a system and scatter model and runs Monte Carlo simulations to calculate the scatter background[3], [4]. However, to get accurate simulation results, large numbers of photons need to be simulated, which leads to long computation times. Other approaches model scatter as a convolution operation using kernels derived using empirical methods. These techniques have been found to be insufficient in spectral CT due to their inability to sufficiently capture object dependence[5].

Recently, deep learning approaches have achieved tremendous success in many fields. In medical imaging for example, there have been extensive research activities applying deep learning. However, most of these efforts are focused on image-based diagnostics[6]. There are a few investigation related to CT imaging[7], [8]. In this work we bring this promising technique into imaging physics. The main goal is to develop a novel deep convolutional neural network (CNN) architecture for scatter correction that approaches the quality of model-based methods with much lower computing costs.

The proposed deep residual learning is based on our conjecture that the scatter distribution of a pencil beam can be determined from its corresponding air-normalized raw signal (primary plus scatter) and the signal in the surrounding area. Therefore, to train the network, the input is a projection with air-normalized raw signal and its label is the corresponding scatter signal, which is calculated in a Monte Carlo simulation. The idea here takes advantage of a residual learning framework where the network learns the small offset scatter signal from the large raw signal.

II. METHODS AND EXPERIMENTS

A. CNN architectures

The very deep ConvNets known as VGG [9] were used for large-scale visual recognition. We change VGG to make it suitable for scatter estimation, and set the depth of the network based on the required receptive field. For model learning, we adopt the residual learning formulation, and incorporate it with batch normalization for fast training and improved performance.

Following the methods in [9], [10], we set the size of the convolution filter to 3x3 but remove all pooling layers.

Therefore, the receptive field of the CNN with depth of d is $(2d + 1) \times (2d + 1)$. We downsample the dimension of each projection to 168 radial detectors and 16 slices. Experimentally, we choose $d = 17$ and we divide each projection with dimension 168×16 into many small patches with dimension 32×16 .

The first convolution layers in our CNN consists of 64 filters of size 3×3 , layers 2-16 each consist of 64 filters of size $3 \times 3 \times 64$, and the last layer consists of a single filter of size $3 \times 3 \times 64$. Except for the first and last layer, each convolution layer is followed by a batch normalization, which is included to speed up training as well as boost performance[10], and rectified linear units (ReLU), which are used to introduce nonlinearity. Simple zero padding is performed in each convolution layer to maintain the correct data dimensions.

The input of our CNN (r) is air-normalized primary signal (p) with additional scatter (s): $r = p + s$. We adopt the residual learning formulation to train a residual mapping $T(r) \sim s$, from which we determine the desired signal $p = r - T(r)$. The CNN parameters are estimated by minimizing the following loss function:

$$L(w) = \sum_j (||T(r; w)_j - s_j||_2^2 + \lambda_1 ||\nabla T(r; w)_j||_1) + \lambda_2 \sum_k ||w_k||_2^2$$

Here w is the set of all convolutional kernels of all layers and $k=1, \dots, 17$ denotes the layer index. The regularization terms encourage a smoothed scatter signal by Total variation constraint [11] and small network kernels. We used the regularization parameters $\lambda_1 = \lambda_2 = 10^{-3}$. Here $\{(r_j, s_j)\}_{j=1}^N$ represents N training pairs of scattered raw signal and scatter-only signal, where j is the index of training unit. The training sets are obtained from MC simulations.

The minimization of the loss function was performed using the conventional error backpropagation with stochastic gradient descent (SGD), where an initial learning rate was set to 0.01, and the learning rate was gradually decreased to 10^{-5} . Mini-batches of size 10 were used, indicating that 10 randomly chosen sets of data were used as a batch. The method was implemented in MATLAB using MatConvNet[12].

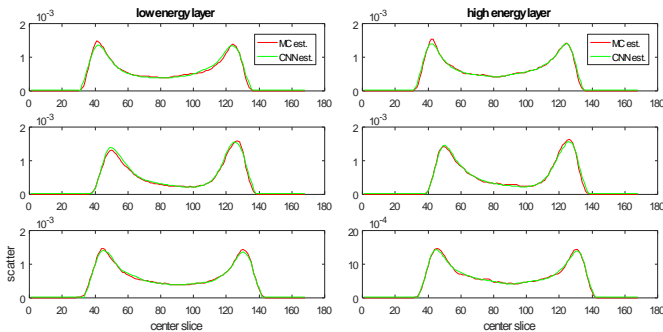


Fig. 1. Scatter profiles from the CNN and from MC (as ground truth) at the center slice for three different views (from top to bottom).

B. Training sets

A model-based Monte Carlo simulation was employed to generate the training sets. The geometry setup and parameters of the simulations were chosen to mimic the characteristics of

the Philips IQon Spectral CT, which has a dual-layer detector. The simulations were performed with a tube voltage of 120 kVp. Three phantoms were used: a 30 cm diameter cylindrical

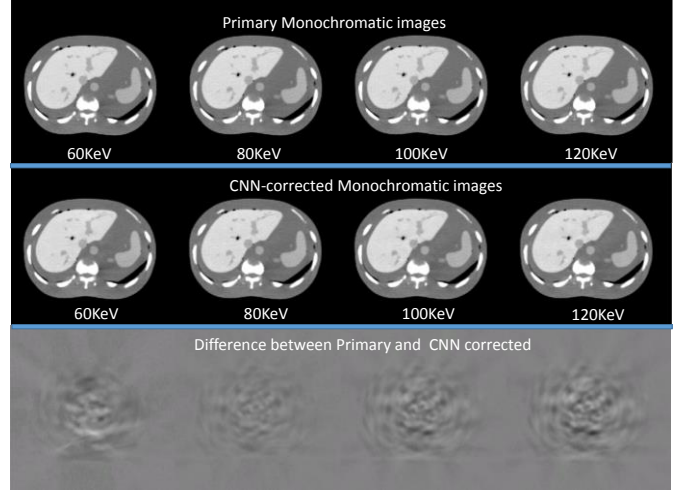


Fig. 2. CNN-corrected monochromatic images ([-50 50]) at 60keV, 80keV, 100keV and 120keV versus Primary monochromatic image ([-50 50]) and their difference [-10 10].

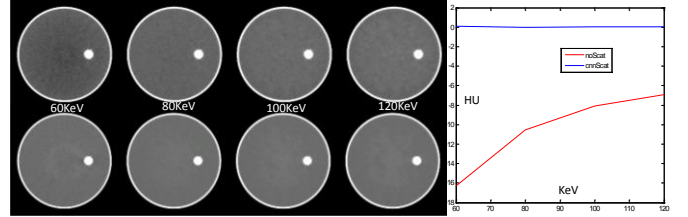


Fig. 3. CNN-corrected monochromatic images ([-50 50]) at 60keV, 80keV, 100keV and 120keV on the top versus monochromatic without scatter correction ([-50 50]) on the bottom. The dispersion curves on the right are drawn by determining the average HU value in the water phantom for each keV, which is supposed to be flat at zero for water across keV.

water phantom, and digital representations of anthropomorphic liver and an obese phantom. For each phantom, the primary signal was determined analytically using 600 (obese and liver) or 2400 (water) projections over a full rotation of 360 degrees. Scatter data was collected by simulating 60 projections over a full rotation with 5×10^8 (water and liver) or 4.5×10^9 (obese) photons per projection. Due to the expensive computation, a limited number of 6 representative scans were used to generate training sets: 1 for the water and obese phantom each and 4 for the liver phantom at different shifts of the phantom in cranio-caudal direction. Data was divided in patches of size 32×16 and augmented by simply flipping along X. The network was trained separately for the low energy layer and the high energy one. The total training time for each layer was about 6 hours on a Dell T7600 workstation with a Titan X GPU.

C. Testing sets

For testing the same liver phantom as above was used but at a cranio-caudal shift that was not used for training. A 30cm water cylinder was used as well but this time scanned on a Philips iQon system, not simulated. We estimated scatter by applying the well-trained network to the low and high-energy signals separately. Scatter correction was performed by simply subtracting the corresponding estimation from the raw data of each layer. The corrected high and low data were then further decomposed into energy independent basis functions, such as

iodine and water. These were reconstructed into basis functions in image space. Monochromatic images were constructed as linear combinations of basis functions.

III. RESULTS

For the simulated data, scatter profiles from the CNN at the center slice of three different views are plotted in Fig. 1, and compared to the those from MC simulation (as ground truth) for both detector layers. After applying the CNN-based scatter correction, monochromatic images at 60keV, 80keV, 100keV and 120keV are reconstructed and compared to the monochromatic images obtained from reconstructing the primary signal, see Fig. 2. For the real water phantom data, we present monochromatic images from 60keV to 120keV, draw dispersion curves, and compare the results with results without scatter correction, see Fig. 3. The computing time to estimate scatter for each projection is about 6-7 ms on the GPU enabled workstation.

IV. CONCLUSION AND DISCUSSION

We developed a deep residual learning framework for scatter correction on spectral CT system. We demonstrated that the proposed method provides similar performance to Monte Carlo simulation-based scatter correction but with a much shorter computing time. The efficacy of the proposed method was also illustrated on real phantom data. We believe that this suggests a new innovative framework to the CT physics field.

References

- [1] T. R. C. Johnson, "Dual-Energy CT: General Principles," *Am. J. Roentgenol.*, 2012.
- [2] R. E. Alvarez and A. Macovski, "Energy-selective reconstructions in X-ray computerized tomography.," *Phys. Med. Biol.*, 1976.
- [3] M. Bertram, J. Wiegert, and G. Rose, "Scatter correction for cone-beam computed tomography using simulated object models," in *Proc. SPIE*, 2006, vol. 6142, p. 61421C.
- [4] a Sisniega, W. Zbijewski, A. Badal, I. S. Kyprianou, J. W. Stayman, J. J. Vaquero, and J. H. Siewerdsen, "Monte Carlo study of the effects of system geometry and antiscatter grids on cone-beam CT scatter distributions," *Med. Phys.*, 2013.
- [5] P. Sainath, X. W. Wu, M. Nukui, R. J. Lundgren, and T. J. Myers, "METHODS AND APPARATUS FOR SCATTER CORRECTION," 2007.
- [6] H. C. Shin, H. R. Roth, M. Gao, L. Lu, Z. Xu, I. Nogues, J. Yao, D. Mollura, and R. M. Summers, "Deep Convolutional Neural Networks for Computer-Aided Detection: CNN Architectures, Dataset Characteristics and Transfer Learning," *IEEE Trans. Med. Imaging*, vol. 35, no. 5, pp. 1285–1298, 2016.
- [7] E. Kang, J. Min, and J. C. Ye, "A deep convolutional neural network using directional wavelets for low-dose X-ray CT reconstruction," pp. 1–29, 2016.
- [8] G. Wang, "A Perspective on Deep Imaging," *IEEE Access*, vol. 4, pp. 8914–8924, 2016.
- [9] K. Simonyan and A. Zisserman, "Very deep convolutional networks for large-scale image recognition," *arXiv Prepr. arXiv1409.1556*, 2014.
- [10] K. Zhang, W. Zuo, Y. Chen, D. Meng, and L. Zhang, "Beyond a Gaussian Denoiser: Residual Learning of Deep CNN for Image Denoising," pp. 1–13, 2016.
- [11] T. Wang, Z. Qin, and M. Zhu, "An ELU Network with Total Variation for Image Denoising," in *arXiv:1708.04317*, 2017.
- [12] A. Vedaldi and K. Lenc, "MatConvNet - Convolutional Neural Networks for MATLAB," *Arxiv*, 2014.